PNAS RESEARCH ARTICLE | NEUROSCIENCE
BIOPHYSICS AND COMPUTATIONAL BIOLOGY OPEN ACCESS

# Interdependence of cellular and network properties in respiratory rhythm generation

Ryan S. Phillips[a,1] and Nathan A. Baertsch[a,b,c,1]

Edited by Eve Marder, Brandeis University Department of Biology, Waltham, MA; received October 27, 2023; accepted March 24, 2024

**How breathing is generated by the preBötzinger complex (preBötC) remains divided between two ideological frameworks, and a persistent sodium current ($I_{NaP}$) lies at the heart of this debate. Although $I_{NaP}$ is widely expressed, the pacemaker hypothesis considers it essential because it endows a small subset of neurons with intrinsic bursting or "pacemaker" activity. In contrast, burstlet theory considers $I_{NaP}$ dispensable because rhythm emerges from "preinspiratory" spiking activity driven by feed-forward network interactions. Using computational modeling, we find that small changes in spike shape can dissociate $I_{NaP}$ from intrinsic bursting. Consistent with many experimental benchmarks, conditional effects on spike shape during simulated changes in oxygenation, development, extracellular potassium, and temperature alter the prevalence of intrinsic bursting and preinspiratory spiking without altering the role of $I_{NaP}$. Our results support a unifying hypothesis where $I_{NaP}$ and excitatory network interactions, but not intrinsic bursting or preinspiratory spiking, are critical interdependent features of preBötC rhythmogenesis.**

spike shape | afterhyperpolarization | respiratory control | rhythm generation | central pattern generation

## Significance

Breathing is a vital rhythmic process originating from the pre-Bötzinger complex. Since its discovery in 1991, there has been a spirited debate about whether respiratory rhythm generation emerges as a network property or is driven by a subset of specialized neurons with rhythmic bursting capabilities, endowed by intrinsic currents. Here, using computational modeling, we propose a unifying, data-driven model of respiratory rhythm generation, which bridges the gap between these competing theories. In this study, we demonstrate that the interaction of cellular (a persistent sodium current) and network properties (recurrent excitation) gives rise to multiple (i.e., degenerate) modes of rhythm generation that are consistent with both theories. Importantly, conditional factors impacting spike shape can promote one mode over the other.

Neural rhythmicity orchestrates critical brain functions and dysregulation of this rhythmicity can lead to pathology. Central pattern generators (CPGs) driving rhythmic functions such as locomotion and digestion are key model systems for investigating brain rhythm generation (1). The mammalian CPG for breathing has been extensively studied as it produces rhythmic motor output that can be measured in awake, anesthetized, and ex vivo experimental preparations. Discovery of the preBötzinger complex (preBötC), a medulla region necessary for respiratory rhythm, inspired the development of preBötC slice preparations (2) that generate rhythm in isolation. These in vitro preparations have been used extensively to identify properties underlying respiratory rhythmogenesis, and computational modeling conducted in parallel has been critical for developing and testing concepts of respiratory rhythmogenesis. Yet, despite rigorous experimental/theoretical investigation, how the preBötC generates rhythm remains controversial (3–5).

The terminology surrounding this controversy has evolved since first being introduced (6). However, the nature of the debate has remained centered on whether cellular- or network-based properties of the preBötC are the essential mechanism of rhythmogenesis. Much of the contemporary debate relates to two competing theories. With its discovery, preBötC neurons were identified that continue to produce rhythmic bursts of action potentials in isolation (2). This finding, inspired the pacemaker hypothesis, which posits that intrinsically bursting or "pacemaker" neurons are a specialized cell type that initiates synchronized activity within the network and represents the essential element of rhythmogenesis. Modeling studies predicted a critical role of a slowly inactivating persistent sodium current ($I_{NaP}$) in the rhythmic activity of pacemaker neurons (7), which was later experimentally confirmed (8). More recently, an alternative view has evolved to account for observations that the amplitude of the preBötC rhythm can be diminished while only minimally affecting its frequency (9–14), suggesting that the network contains dissociable rhythm and "burst" generating elements (3, 15). One interpretation of these results is conceptualized as burstlet theory (3), based on the preceding "group pacemaker" hypothesis (6), which proposes that rhythm is driven by weakly synchronized spiking activity referred to as "burstlets" that are an emergent property of preBötC network topology and feed-forward excitatory synaptic interactions among a subset of nonpacemaker neurons. Thus, in burstlet theory, ramping spiking activity prior to inspiratory bursts referred to as "preinspiratory spiking" represents burstlets and the essential rhythmogenic element of the network, while intrinsic bursting neurons and associated burst-promoting conductances including $I_{NaP}$ are considered dispensable (3, 9, 16).

Author contributions: R.S.P. designed research; R.S.P. performed research; R.S.P. analyzed data; and R.S.P. and N.A.B. wrote the paper.

The authors declare no competing interest.

This article is a PNAS Direct Submission.



[1]To whom correspondence may be addressed. Email: Ryan.Phillips@seattlechildrens.org or Nathan.Baertsch@seattlechildrens.org.

This article contains supporting information online at https://www.pnas.org/lookup/suppl/doi:10.1073/pnas.2318757121/-/DCSupplemental.

Published May 1, 2024.

However, both theories are difficult to test and overlook the possibility that there may be degenerate modes through which cellular activity can give rise to a network rhythm. Further, the validity of both theories remains unclear due to conflicting findings and oversimplifications that have hindered progress toward a consensus on how breathing originates. Initially, the pacemaker hypothesis was widely adopted due to its simplicity and convincing experimental (2, 8, 17, 18) and theoretical (7, 19, 20) support. However, demonstrating that intrinsic bursting neurons are critical for rhythmogenesis proved to be far from simple. First, intrinsic bursting neurons are difficult to identify, typically requiring blockade of synaptic network interactions rendering the network nonfunctional. Second, intrinsic bursting neurons cannot be specifically manipulated to define their functional role. For example, although $I_{NaP}$ is higher on average in intrinsic bursters, $I_{NaP}$ is widely expressed in the preBötC in both intrinsically bursting and nonbursting neurons (8, 18, 21). Because of this ubiquitous expression, manipulations of $I_{NaP}$ are not specific to intrinsic bursting neurons making it difficult or impossible to characterize their specific contribution to rhythmogenesis. Third, intrinsic bursting does not appear to be a fixed property since neurons may be capable of bursting in some conditions, but not in others (22). For instance, when challenged with hypoxia, the preBötC network produces a gasping-like rhythm with enhanced sensitivity to $I_{NaP}$ blockade (23) and is associated with a loss of preinspiratory spiking, inconsistent with the rhythmogenic mechanism proposed by burstlet theory. On the other hand, identification of preBötC pacemaker neurons has relied on ex vivo preparations from neonatal mice with associated caveats such as elevated extracellular $K^+$ and low temperature (2), while there remains a lack of evidence for intrinsically bursting preBötC neurons in adult animals in vivo, casting doubt on the pacemaker hypothesis (3).

Here, we develop a model of respiratory rhythmogenesis that accounts for these discrepancies, while remaining constrained by experimental findings that support both the pacemaker hypothesis and burstlet theory. Due to interactions with the voltage-dependent properties of $I_{NaP}$, we find that small changes in spike shape, without changes in $I_{NaP}$ or excitability, can eliminate the capability of model neurons to exhibit intrinsic bursting. By exploiting this interaction to dissociate the functional roles of $I_{NaP}$ and intrinsic bursting, we find that model preBötC networks comprised entirely of neurons rendered incapable of intrinsic bursting continue to produce rhythm. In this extreme case, excitatory synaptic interactions allow rhythm to emerge among tonic neurons that typically exhibit preinspiratory spiking in the synaptically coupled network. Yet, despite the absence of intrinsic bursting, the network rhythm remains dependent on $I_{NaP}$. At the other extreme, in networks with spike shapes that render all neurons capable of intrinsic bursting, rhythmogenesis continues despite minimal preinspiratory spiking. In this case, the network rhythm also depends on $I_{NaP}$ as well as excitatory interactions that synchronize intrinsic bursting to produce a coherent network rhythm. Introducing spike shape variability allows subsets of neurons to regain intrinsic bursting capabilities or preinspiratory spiking, but this does not endow them with an essential role in rhythm generation per se. Instead, the interdependence of $I_{NaP}$ and excitatory synaptic interactions represents the critical substrate for rhythmogenesis, while intrinsic bursting and preinspiratory spiking are conditional phenotypes of preBötC neurons that reflect degenerate modes of rhythm generation, sensitive to any perturbation that affects spike shape including, but not limited to, extracellular $K^+$, temperature, hypoxia, and neurodevelopment. These findings support a unifying theory of respiratory rhythm generation and may also provide a useful framework for understanding the emergence of rhythmicity in other brain networks.

## Results

**Spike Shape Regulates Intrinsic Bursting.** Spike shapes vary widely, and in the preBötC spike amplitudes range from approximately 15 to 125 mV (20, 24, 25). Due to the voltage-dependence of $I_{NaP}$ (in)activation (8, 18, 21), we wondered whether spike shape could impact intrinsic bursting. To selectively manipulate spike shape, we incorporated two additional currents, $I_{SPK}$ and $I_{AHP}$, into a contemporary preBötC neuron model (15), (Fig. 1*A*). The voltage-dependent properties of $I_{SPK}$ and $I_{AHP}$ (in)activation were chosen such that they are only active well above resting membrane potential (≈-27.5mV), allowing selective control of spike shape without affecting excitability. Although these currents are not intended to mimic any of the numerous channels expressed in the preBötC that may influence spike shape (25), the voltage-dependence of $I_{SPK}$ and $I_{AHP}$ are

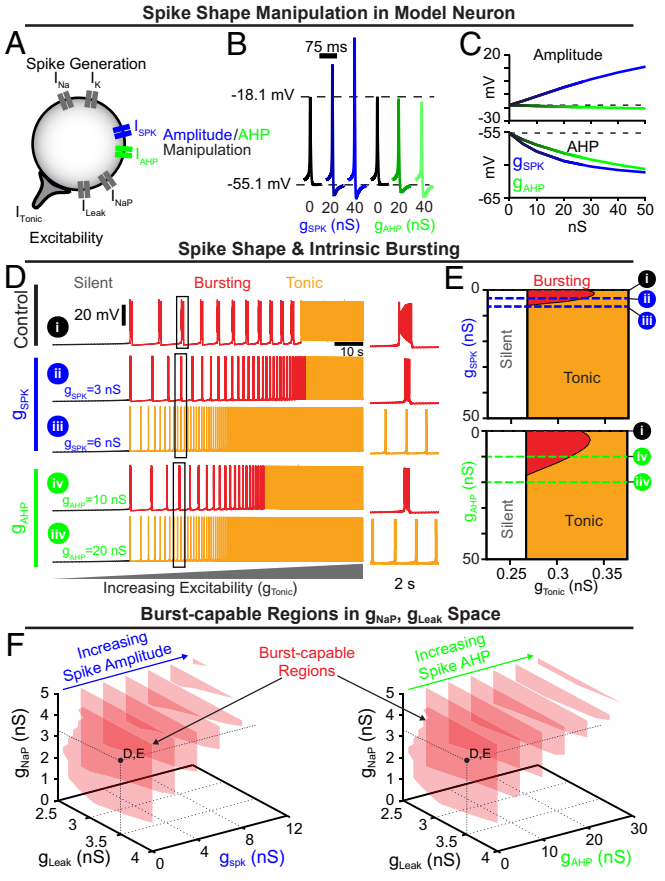


**Fig. 1.** Spike shape regulates $I_{NaP}$-dependent intrinsic bursting. (*A*) Schematic diagram of a model neuron with modifiable spike shape. (*B*) Example spike shapes and (*C*) quantification of spike amplitude and AHP during increasing $g_{SPK}$ or $g_{AHP}$. (*D*) Voltage traces of an average intrinsic burster $g_{NaP}$ = 3.33 nS and $g_{leak}$ = 3.5 nS (18) illustrating how increasing $g_{SPK}$ or $g_{AHP}$ changes the activity pattern (silent, bursting, or tonic) produced as $g_{Tonic}$ is varied. (*E*) Activity patterns as a function of $g_{Tonic}$ and $g_{SPK}$ (*Left*) or $g_{AHP}$ (*Right*). Notice that for small increases in $g_{SPK}$ or $g_{AHP}$, intrinsic bursting (red shaded region) is lost and the neuron is rendered "burst-incapable." (*F*) Burst-capable regions (transparent red) in $g_{Leak}$, $g_{NaP}$ space as a function of $g_{SPK}$ (*Left*) or $g_{AHP}$ (*Right*). Black dots indicate $g_{Leak}$, $g_{NaP}$ values used in *D* and *E*.

similar to NaV1.2 (26) and noninactivating M-currents, that are expressed by preBötC neurons (21). For a full description see Materials and Methods. As expected, increasing the $I_{SPK}$ conductance ($g_{SPK}$) increased spike amplitude by ≈30 mV (−18.1 mV to +11.2 mV) over the range of conductances tested (0 to 50 nS). Over the same range of $g_{SPK}$, the magnitude of the spike afterhyperpolarization (AHP) was also increased by ≈6 mV (−55.1 mV to −61.1 mV). In contrast, increasing the $I_{AHP}$ conductance ($g_{AHP}$) from 0 to 50 nS had a more selective effect on spike AHP, increasing it from −55.1 to −60.6 mV with minimal changes in spike amplitude (Fig. 1 *B* and *C*).

To characterize the interaction between spike shape and intrinsic bursting, we altered $g_{SPK}$ or $g_{AHP}$ in model neurons with experimentally motivated $I_{NaP}$ conductance ($g_{NaP}$) (8, 18) while manipulating excitability via a tonic excitatory conductance ($g_{Tonic}$). Importantly, intrinsic bursting is voltage-dependent as illustrated in Fig. 1 *D*, Top where the model neuron transitions from silent, to intrinsic bursting (periodic bursts of spiking), and then to tonic spiking (continuous spiking) as excitability increases (2, 7, 8, 18). Surprisingly, small increases in spike amplitude or AHP rapidly reduced the range of excitability ($g_{Tonic}$) where intrinsic bursting was possible, followed by complete elimination of intrinsic bursting capabilities at $g_{SPK}$ = 5.816 nS or $g_{AHP}$ = 17.143 nS corresponding to changes in spike amplitude or AHP of approximately +3.5 mV and −3.0 mV, respectively (Fig. 1 *D* and *E*). Specifically, as spike amplitude or AHP increased, the number of spikes and their frequency during bursts decreased until the neuron transitioned to tonic spiking (Fig. 1*D* and *SI Appendix*, Fig. S1). Importantly, following these changes in spike shape, neurons remained unable to generate intrinsic bursting at all levels of excitability, transitioning directly from silent to tonic spiking, which we refer to here as being "burst-incapable." In addition to $g_{NaP}$, the potassium-dominated leak conductance ($g_{Leak}$) is an important determinant of intrinsic bursting and varies among preBötC neurons (8, 18). Therefore, we mapped burst capability across $g_{NaP}$,$g_{Leak}$ parameter space during manipulations of spike shape (Fig. 1*F*). As $g_{SPK}$ or $g_{AHP}$ were increased, the burst-capable region collapsed toward higher $g_{NaP}$ and lower $g_{Leak}$ values until intrinsic bursting became impossible at $g_{SPK}$ >13nS or $g_{AHP}$ >35nS. Thus, even model neurons with high $g_{NaP}$ and low $g_{Leak}$ require spike shape to be maintained within a certain range to be capable of intrinsic bursting.

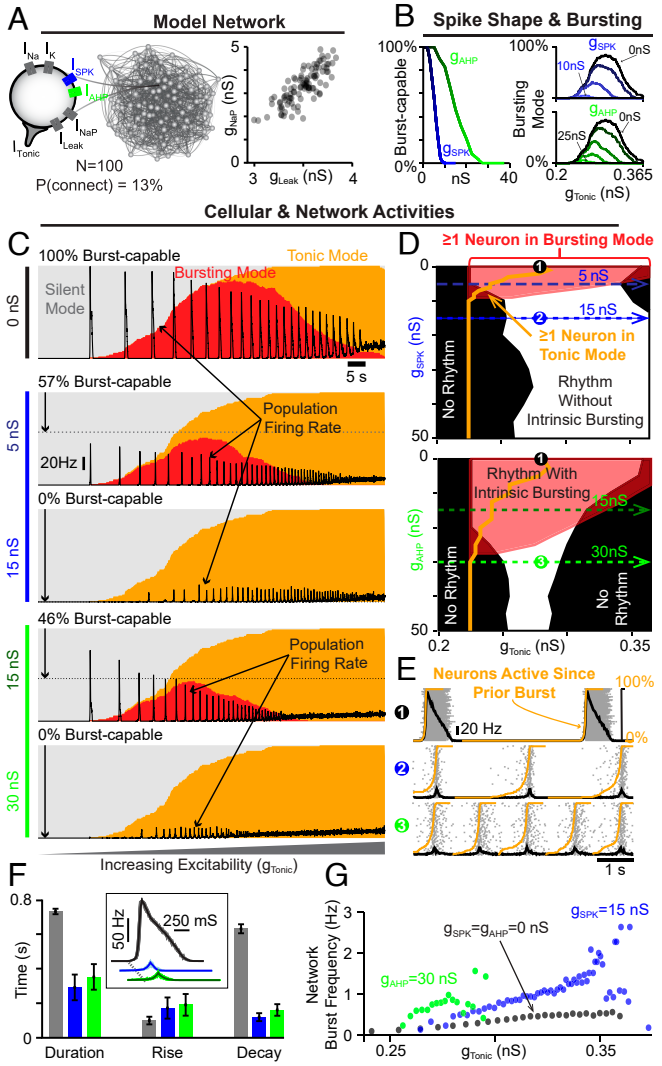


**Fig. 2.** Rhythm generation continues despite loss of intrinsic bursting. (*A*) Schematic of 100 neuron network and the $g_{NaP}$ and $g_{Leak}$ distribution within the network. (*B*) Percentage of burst-capable neurons in the network as a function of $g_{SPK}$ or $g_{AHP}$ and (*Right*) the relationship between $g_{Tonic}$ and the percentage of the population in bursting mode during increasing $g_{SPK}$ or $g_{AHP}$. Effects of increasing (*C*) $g_{SPK}$ or $g_{AHP}$ on the network activity (firing rate, black traces) and intrinsic cellular activity modes (silent, bursting, tonic) as excitability is increased and (*D*) corresponding parameter space supporting intrinsic bursting (red), tonic spiking (orange lines), and network rhythmogenesis (white). Dashed blue and green lines correspond to $g_{SPK}$/$g_{AHP}$ and ramp in $g_{Tonic}$ used for the example traces shown in the *C*. (*E*) Example raster plots with overlaid population firing rate for each condition at a fixed $g_{Tonic}$. (*F*) Quantification of burst duration, rise, and decay times. The *Inset* shows cycle-triggered averages of network burst waveforms. (*G*) Effect of increasing $g_{SPK}$ or $g_{AHP}$ on the range of possible network burst frequencies.

**Intrinsic Bursting Is not Required for preBötC Network Rhythmogenesis.** Testing whether intrinsic bursting or "pacemaker" neurons are critical for preBötC rhythmogenesis has been difficult/controversial (*Introduction*) and can be misleading considering degeneracy (1). Therefore, we leveraged the interaction between spike shape and intrinsic bursting to investigate how manipulation of intrinsic bursting, without associated changes in $I_{NaP}$ or excitability, impacts rhythm generation in a network of *N* = 100 model neurons (Fig. 2*A*). See *Material and Methods* for a full description.

Because these model networks contain neurons with distributed $g_{NaP}$ and $g_{Leak}$ values (Fig. 2*A*), we characterized how increasing spike amplitude and/or spike AHP impacts intrinsic bursting capabilities across the population. Under control spike shape conditions ($g_{SPK}$ = $g_{AHP}$ = 0 nS), all neurons were initially burst-capable. However, due to the spike shape dependence of intrinsic bursting, increasing $g_{SPK}$ or $g_{AHP}$ progressively rendered neurons burst incapable, with low $g_{NaP}$ neurons being the most susceptible. When spike amplitude was increased by as little as ≈10 mV ($g_{SPK}$ = 10 nS) or the AHP was increased by ≈4 mV ($g_{AHP}$ = 30 nS), the intrinsic bursting capabilities of all neurons in the population were eliminated (Fig. 2*B*).

Next, we examined network activity relative to the intrinsic activity modes (silent, bursting, tonic) of its constituent neurons. This was done by determining the percentage of neurons that are silent, bursting, or tonic in the absence of synaptic interactions as a function of excitability ($g_{Tonic}$) (Fig. 2 *B* and *C*). Excitatory synaptic interactions were then introduced, and population firing rate over the same excitability range was overlaid (black traces) with intrinsic activity modes (gray, red, and orange shaded areas) to compare cellular- and network-level characteristics (Fig. 2*C*).

Under control spike shape conditions (100% burst-capable), as excitability was increased the percentage of neurons in bursting mode increased and then decreased as neurons transitioned to tonic mode. This revealed a bell-shaped curve where the maximum number of neurons in bursting mode was always less than the number of burst-capable neurons, which occurs due to the distributed $g_{NaP}$, $g_{Leak}$ parameters of each neuron. Following introduction of synaptic connections, the control network produced a rhythm that followed this bell-shaped curve, beginning as soon as the first neuron entered an intrinsic bursting mode and ending once most neurons switched to tonic mode (black trace vs. red shaded area in Fig. 2*C*). In model networks with altered spike shape, the bell-shaped curve of neurons in bursting mode was initially reduced, involving a smaller percentage of the network and occurring over a narrower range of excitability, and then eliminated once all neurons were rendered burst-incapable at $g_{SPK}$ ≈10 nS or $g_{AHP}$ ≈30 nS (Fig. 2*D*). Consequently, as excitability was increased, neurons transitioned directly from silent to tonic modes. Surprisingly, the network still became rhythmic once a sufficient fraction of neurons (≈15%) entered tonic mode. Thus, contrary to the pacemaker hypothesis and the expected mechanism of rhythm generation in similar $I_{NaP}$-based model networks (14, 15, 19, 20, 27), intrinsic bursting is not required for rhythm generation.

Changes in spike shape also affected network spiking activity (Fig. 2*E*). Altering either spike shape feature slowed the firing rate of individual neurons during bursts to ≈20 Hz, reducing the network rhythm amplitude. These rhythms may appear relatively weak but are more representative of preBötC activity. First, the large amplitude rhythm under control conditions is associated with firing rates reaching >130 Hz in many neurons, but firing rates of preBötC neurons during bursts typically range from very slow (<5 Hz) to a maximum near ≈50 Hz (17, 28). Second, increasing $g_{SPK}$ or $g_{AHP}$ converted network bursts from a decrementing pattern to one with roughly symmetrical rise and decay times of ≈150 to 200 ms (Fig. 2*F*), consistent with typical preBötC activity as well as the cellular and network level dynamics of burstlets (3, 29). Third, modifying spike shape at a given level of $g_{Tonic}$ increased the fraction of neurons in the network that began to spike prior to burst onset, resulting in a collective "preinspiratory" ramping of network activity (orange lines in Fig. 2*E*). This preinspiratory spiking reflects the recovery of activity in neurons in tonic spiking mode (*SI Appendix*, Fig. S2), as previously suggested (19, 30).

Notably, manipulating spike shape altered how the network rhythm responded to changes in excitability. Specifically, the $g_{Tonic}$ range supporting rhythmogenesis was shifted slightly with increasing $g_{SPK}$ and reduced with $g_{AHP}$, (Fig. 2*G*), which could be mitigated by increasing synaptic strength (*SI Appendix*, Fig. S3). Yet, despite this reduced excitability "window," the network responsiveness to changes in $g_{Tonic}$ was enhanced such that the dynamic range of possible burst frequencies increased by two to three fold. Overall, these results demonstrate that 1) network rhythmogenesis persists even in the extreme case when all neurons are rendered incapable of intrinsic bursting, 2) reducing the number of burst-capable neurons without altering $I_{NaP}$ produces a rhythm with spiking patterns that are more representative of preBötC activity, and 3) modulation of spike shape can change the gain of the network rhythm such that it responds with a greater change in frequency to a given excitatory input.

**Interdependence of $I_{NaP}$ and Excitatory Synaptic Dynamics.** Our finding that rhythmogenesis continues without intrinsic bursting was surprising since $I_{NaP}$-based computational models of the preBötC are generally viewed as the embodiment of the pacemaker hypothesis. In other preBötC models that lack $I_{NaP}$ and intrinsic bursting, specialized synaptic dynamics (depression/facilitation) are required for network oscillations (31, 32). Similarly, synapses in our preBötC model undergo activity-dependent synaptic depression (15). Therefore, to understand what underlies network rhythmogenesis in the absence of intrinsic bursting, we blocked $I_{NaP}$ or removed synaptic depression under control conditions (100% burst-capable, $g_{SPK}$ = $g_{AHP}$ = 0 nS) and following elimination of intrinsic bursting via increased spike amplitude and/or AHP ($g_{SPK}$ = 15 nS or $g_{AHP}$ = 35 nS). In all conditions, the network rhythm continued when synaptic depression was turned off, with modestly increased burst duration and decreased burst frequency (Fig. 3*A* & *SI Appendix*, Fig. S4). Thus, although synaptic depression may have important effects on rhythm characteristics, its elimination does not preclude rhythmogenesis. To test the role of $I_{NaP}$, we set $g_{NaP}$ = 0 nS to eliminate its activity from all neurons in the network. As expected, under all conditions removing $I_{NaP}$ decreased neuronal excitability resulting in higher levels of $g_{Tonic}$ required to drive spiking activity. However, all networks remained unable to generate rhythm even as $g_{Tonic}$ was increased to restore excitability to levels producing comparable spike rates (*SI Appendix*, Fig. S4). For comparison, networks with synapses blocked ($g_{syn}$ = 0 ns) were also unable to produce rhythm at any level of excitability, illustrating the somewhat trivial but important point that synaptic interactions are always a requirement for network rhythm, even if all neurons are intrinsic bursters. These results demonstrate that $I_{NaP}$ can remain a critical component of the rhythmogenic mechanism beyond its contribution to network excitability and

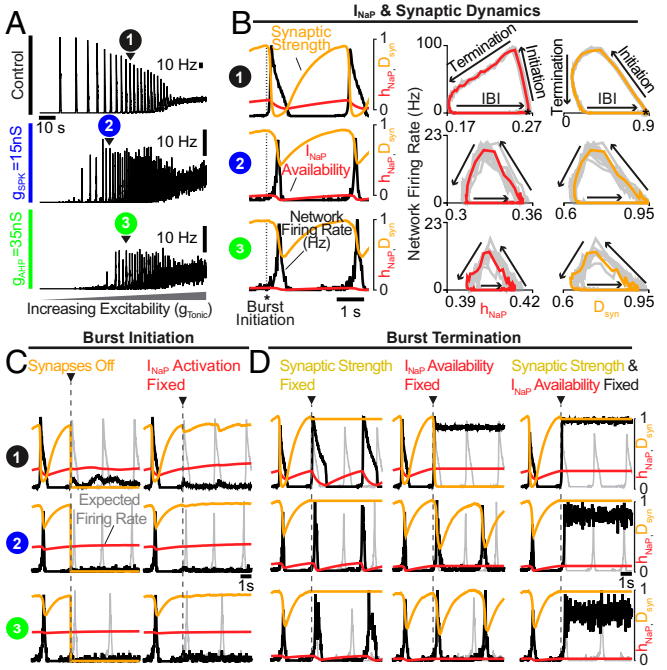


**Fig. 3.** Interdependence of $I_{NaP}$ and synaptic interactions for network rhythmogenesis. (*A*) Activity of networks with all burst-capable (control) or burst-incapable ($g_{SPK}$ = 15 nS or $g_{AHP}$ = 35 nS) neurons. (*B*) Relationship between network firing rate, $I_{NaP}$ availability, and synaptic strength during network burst initiation, termination, and the interburst interval. (*C*) Network activity when synapses are turned off (*Left*) or $I_{NaP}$ activation ($m_{NaP}$) is fixed in neurons that have not yet spiked (*Right*) at burst initiation. (*D*) Network activity when synaptic strength (*Left*), $I_{NaP}$ availability ($h_{NaP}$, *Middle*), or both (*Right*), are fixed at burst initiation. Gray traces indicate expected network activity.

independent of whether preBötC neurons are capable of intrinsic bursting.

Next, we performed phase-specific manipulations of $I_{NaP}$ activation ($m_{NaP}$), availability/inactivation ($h_{NaP}$), and/or synaptic dynamics. In control networks and following spike shape manipulations to eliminate intrinsic bursting ($g_{SPK}$ = 15 nS or $g_{AHP}$ = 35 nS), $I_{NaP}$availability and synaptic strength evolve with network firing rate along similar rotational trajectories during the respiratory cycle, comprised of burst initiation, burst termination, and the interburst interval (Fig. 3*B*). First, synaptic strength/depression ($D_{Syn}$) or $I_{NaP}$ activation were manipulated at burst initiation (Fig. 3*C*). In all cases, when synapses were turned off at burst initiation, the expected network burst did not materialize, indicating that excitatory synaptic interactions are required to transition the network into bursts, even when all neurons are capable of intrinsic bursting and were synchronized by the previous cycle. Similarly, if $I_{NaP}$ activation was fixed at burst initiation, the network burst failed to occur under all conditions. Thus, with impaired $I_{NaP}$ activation, synaptic interactions cannot initiate network bursts, and vice versa, illustrating that these can be interdependent properties of rhythmogenesis. Next, we characterized the role of synaptic depression and $I_{NaP}$availability dynamics in burst termination (Fig. 3*D*). Under all conditions, synaptic depression was not essential for burst termination. However, without it burst duration was increased and the subsequent burst was delayed, particularly in the control network when all neurons were burst-capable. Interestingly, when $I_{NaP}$availability was fixed at burst initiation, network bursts only failed to terminate in control networks. In contrast, in networks lacking intrinsic bursting, fixing $I_{NaP}$availability at burst initiation did not prevent burst termination. Instead, interburst intervals became irregular (*SI Appendix*, Fig. S5), possibly indicative of a more stochastic process of burst initiation (3, 29). Finally, if synaptic depression and $I_{NaP}$availability were both fixed at burst initiation, bursts failed to terminate under all conditions. These results demonstrate that $I_{NaP}$ inactivation and/or synaptic depression can terminate network bursts with neither being independently essential, representing degenerate features of burst termination and exemplifying the limitations of necessity criterion.

**PreBötC Rhythmogenesis Is Robust to Partial $I_{NaP}$ Block.** The effects of $I_{NaP}$ antagonists on the preBötC rhythm have been inconsistent, fueling the debate surrounding the role of $I_{NaP}$ (*Discussion*). Therefore, our model's prediction that $I_{NaP}$ is an essential element for preBötC rhythm-generation may seem controversial. This is due, in part, to the conflation of $I_{NaP}$ with intrinsic bursting and the observation that $I_{NaP}$-dependent intrinsic bursting is more sensitive to pharmacological manipulations than the network rhythm (9, 14). To test this in our model, we examined how the network rhythm and intrinsic bursting are affected by progressive attenuation of $I_{NaP}$. Because the spike shape configurations described above represent the extreme scenarios (100% and 0% burst-capable), we simulated $I_{NaP}$ blockade in networks where $g_{SPK}$ was increased to 6 nS or uniformly distributed from 0 to 12 nS ($g_{SPK}$ = U(0,12) nS), reducing the fraction of burst-capable neurons to 38% and 37%, respectively (6). Since effects of progressive $I_{NaP}$ block were similar, simulations with $g_{SPK}$ = U(0,12) nS, $g_{SPK}$ = 15 nS, $g_{AHP}$ = 35 nS, and $g_{SPK}$ = $g_{AHP}$ = 0 nS are shown in (*SI Appendix*, Figs. S6 and S7). With $g_{SPK}$ = 6 nS (Fig. 4 *A* and *B*), progressive $I_{NaP}$ blockade quickly reduced the fraction of burst-capable neurons and eliminated all intrinsic bursting when $g_{NaP}$ was reduced by just ≈35% (Fig. 4 *C1–E1*). Remarkably, much higher levels of $I_{NaP}$ block were needed to prevent network rhythmogenesis, requiring $g_{NaP}$ to be reduced by ≈80 to 90% (white vs. red regions of Fig. 4*E1*). Furthermore, effects were dependent on the excitability of the network prior to $I_{NaP}$ block, with lower excitability networks being more sensitive to $I_{NaP}$ block and higher excitability networks being less sensitive (compare points 1 to 5 in Fig. 4 *E1* and *F1*). Notably, if the rhythm was stopped by partial blockade of $I_{NaP}$, an $I_{NaP}$-dependent rhythm could be restored by increasing network excitability. These simulations illustrate how slightly different experimental conditions that influence preBötC excitability could lead to surprisingly variable results during pharmacological attenuation of $I_{NaP}$ and different interpretations regarding its role in rhythm generation.

Because $I_{NaP}$ is not specific to intrinsic bursting neurons, making their selective manipulation experimentally intractable, we leveraged the advantages of computational modeling to compare the role of $I_{NaP}$ in burst-capable and burst-incapable neurons. In networks with $g_{SPK}$ = 6 nS (Fig. 4 *C2–F3*) or $g_{SPK}$ = U(0,12) nS (*SI Appendix*, Fig. S7 *C2–F3*) selective suppression of $I_{NaP}$ by only ≈35% in neurons that were initially burst-capable (38% of the network) eliminated all intrinsic bursting from the network. In contrast, selective suppression of $g_{NaP}$ in burst-incapable neurons (62% of network) had no effect on the prevalence of intrinsic bursting, which remained constant at 38%. However, despite dramatically different effects on the prevalence of intrinsic bursting, selective block of $I_{NaP}$ in burst-capable or burst-incapable populations led to similar reductions in total $I_{NaP}$ in the network (47% and 53%, respectively) and had surprisingly similar effects on network rhythmogenesis; further demonstrating that intrinsic bursting does not play an essential role in $I_{NaP}$-dependent network rhythm generation, and highlighting the degenerate modes of rhythm generation in these circuits.

**Dynamic Regulation of Intrinsic Bursting and Preinspiratory Spiking via Small Conditional Modifications in Spike Shape.** The manipulations of spike shape in the initial simulations (Figs. 1–4) were imposed. However, spike shape is dynamically regulated and is altered by numerous conditional factors including e.g. temperature (33, 34), oxygenation (35), intra/extracellular ion concentrations (36, 37), and neurodevelopment (38, 39). Deliberate manipulations of these conditional factors appears to affect preBötC intrinsic bursting (20, 23, 34, 40). These factors also represent variables that are likely to differ between individual experiments and different research groups. Therefore, we explored whether indirect effects on spike shape during simulated changes in 1) oxygenation, 2) neurodevelopment, 3) extracellular potassium, and 4) temperature could capture experimental observations and provide conceptual insights into how conditional regulation of intrinsic bursting may obscure its perceived role in respiratory rhythmogenesis.

***Hypoxia Mediated Changes in Spike Generation, Intrinsic Bursting, and Network Dynamics.*** The preBötC exhibits a biphasic response to acute hypoxia, with augmented followed suppressed network activity and a transition to a slow gasping-like rhythm that appears more reliant on $I_{NaP}$-dependent intrinsic bursting (23). In hypoxia, ATP production is decreased, which impairs $Na^+/K^+$-ATPase pump function and disrupts ion gradients particularly intracellular sodium ($[Na^+]_{in}$) (41). Consequently, spike-generating currents are weakened, and spike amplitude and AHP are reduced (35), which should increase the prevalence of

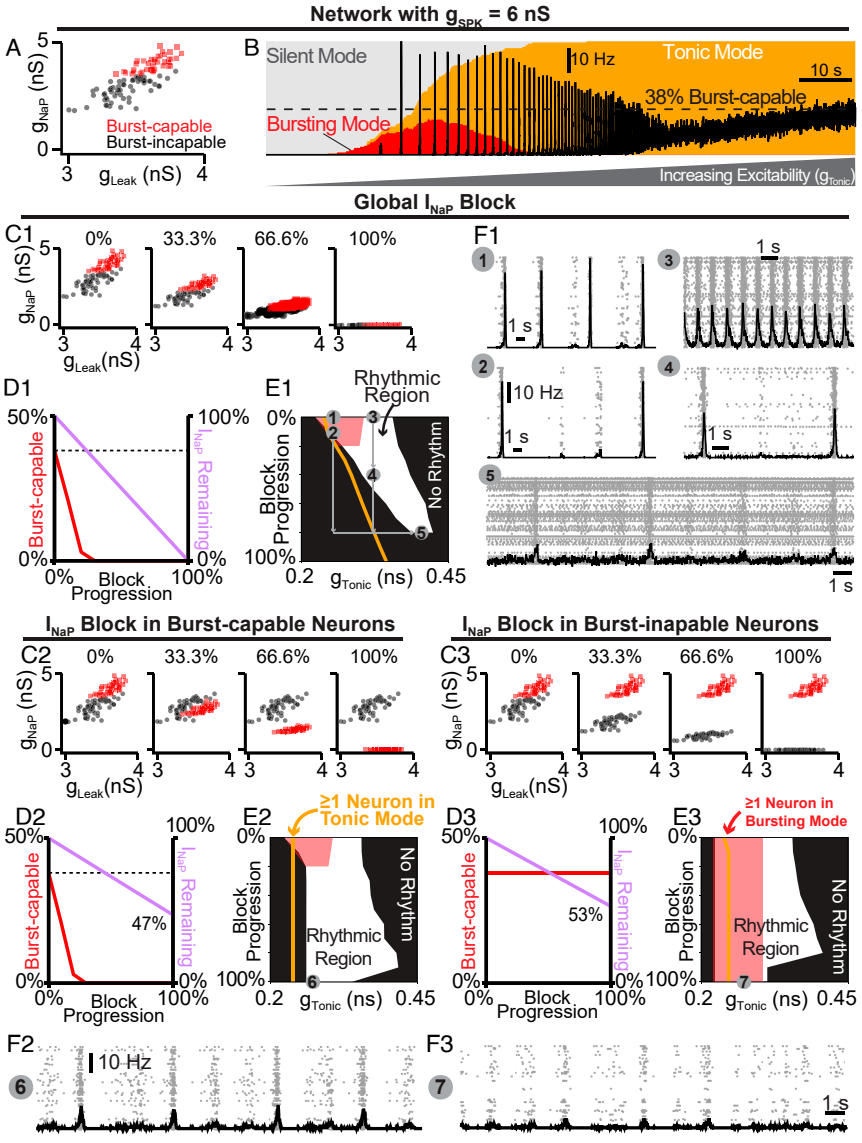


**Fig. 4.** Selective block of $I_{NaP}$ in burst-capable or burst-incapable neurons has similar consequences for rhythm generation. (*A*) Distributions of $g_{NaP}$ and $g_{Leak}$ among burst-capable (red) and incapable (black) neurons in a network with $g_{SPK}$ = 6 nS. (*B*) Prevalence of silent, bursting, and tonic intrinsic cellular activities with overlaid network firing rate during increasing $g_{Tonic}$ in the same network. (*C1–C3*) Comparison of global $I_{NaP}$ block (*C1*) vs. progressive $I_{NaP}$ block specifically in neurons that are initially burst-capable (*C2*) or burst-incapable (*C3*). (*D1–D3*) Fraction of the network that is burst-capable and amount of $I_{NaP}$ remaining as a function of $I_{NaP}$ block progression. (*E1–E3*) Parameter space supporting intrinsic bursting (red) and network rhythmogenesis (white) as a function of excitability ($g_{Tonic}$) during progressive $I_{NaP}$ block. (*F1–F3*) Raster plots and overlaid network firing rate corresponding to points 1 to 7 shown in *E1–E3*.

intrinsic bursting (Fig. 1). However, $[Na^+]_{in}$ accumulation also affects $I_{NaP}$, making its impact on intrinsic bursting unclear.

Therefore, we investigated how elevated $[Na^+]_{in}$ impacts spike shape, intrinsic bursting, and network dynamics. In the single-neuron model, increasing $[Na^+]_{in}$ decreased the sodium reversal potential and negligibly decreased the leak reversal potential (*SI Appendix*, Fig. S8 *A* and *B*), leading to reduced spike amplitude and AHP (Fig. 5 *A* and *B*). Increasing $[Na^+]_{in}$ also reduced neuronal excitability as indicated by higher levels of $g_{Tonic}$ required to generate spiking/bursting (Fig. 5*C*). Despite reduced spike amplitude and AHP, in model networks with distributed $g_{SPK}$ (U(0,12) nS), the percentage of burst-capable neurons slightly decreased with elevated $[Na^+]_{in}$ (Fig. 5*D*) due to the concurrent weakening of $I_{NaP}$. In the neurons that remained burst-capable, bursts duration increased with higher firing rates (Fig. 5 *D*, *Insets*). In the coupled network, increasing $[Na^+]_{in}$ decreased burst frequency and slightly increased amplitude before the rhythm was eventually lost at $[Na^+]_{in}$ >21 mM (Fig. 5*E*).

Increasing $[Na^+]_{in}$ alone did not capture the initial augmenting phase of the hypoxic response. It was recently demonstrated that the initial depolarization of neurons in response to hypoxia is due to rapid (within 40 s) hyperpolarization of the voltage-dependent activation of fast spike-generating sodium channels (26). Accordingly, we tested how hyperpolarizing $I_{Na}$ activation ($V_{1/2}^{Na}$ = − 43.8 mV) (*SI Appendix*, Fig. S8*C*) impacts spike-generation, intrinsic bursting, and network dynamics. Unexpectedly, in single neurons, neither spike amplitude nor AHP was significantly affected (Fig. 5*F*). However, the spike "threshold" was lowered (Fig. 5*G*) increasing neuronal excitability, as indicated by a reduction in the level of $g_{Tonic}$ required to depolarize neurons into tonic or bursting modes (Fig. 5*H*). Additionally, as $V_{1/2}^{Na}$ was hyperpolarized, the number of burst-capable neurons increased from 37% to 67% at $\Delta V_{1/2}^{Na}$ = −1.5 mV and burst duration increased with higher firing rates (Fig. 5*I*). In the model network, hyperpolarizing $V_{1/2}^{Na}$ by 1 mV over 40 s led to an initial increase in network burst frequency followed by elimination of the rhythm (Fig. 5*J*).

Finally, we simulated the combined effects of altered $V_{1/2}^{Na}$ and elevated $[Na^+]_{in}$. In the single neuron model with $[Na^+]_{in}$ = 47.5 mM and $\Delta V_{1/2}^{Na}$ = −1 mV, spike amplitude and AHP were reduced by ≈7.5 mV and ≈1.4 mV, respectively (Fig. 5*K*) and

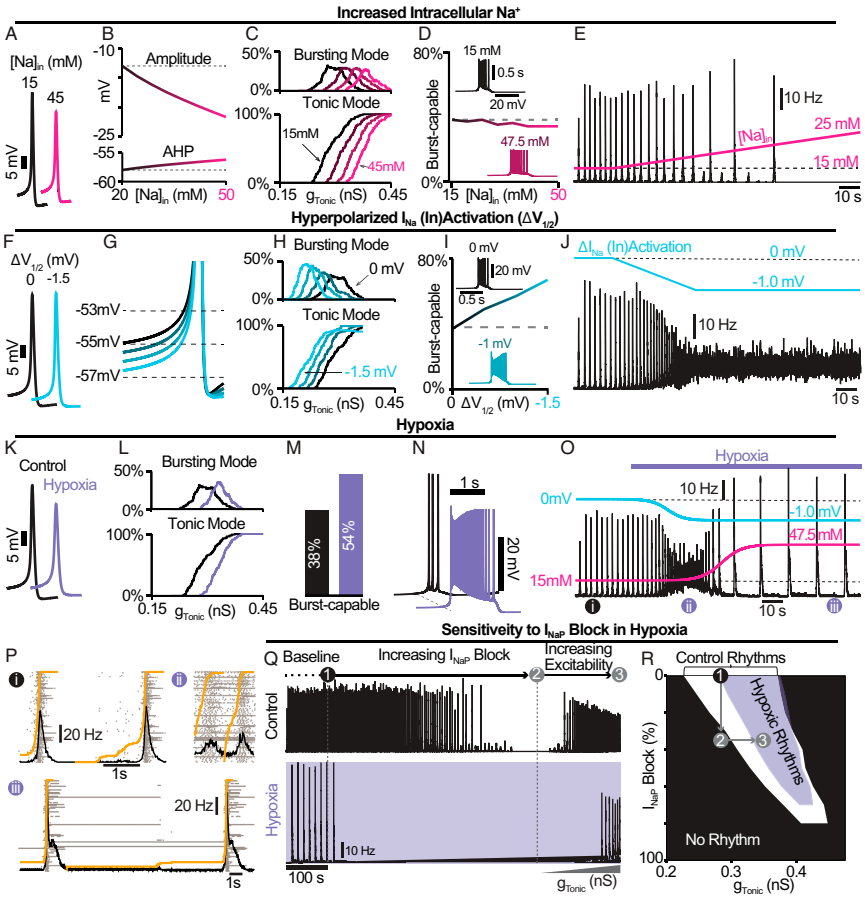


**Fig. 5.** Simulated hypoxia alters spike generation, intrinsic bursting, network dynamics. (*A*) Example traces and (*B*) quantification of spike amplitude and AHP during changes in $[Na^+]_{in}$. (*C*) Relationship between $g_{Tonic}$ and the percentage of the network in tonic or bursting modes showing decreased excitability during elevated $[Na^+]_{in}$. (*D*) Number of burst-capable neurons in the network as a function of $[Na^+]_{in}$ with insets illustrating the impact on burst shape. (*E*) Effect of increasing $[Na^+]_{in}$ on the model network rhythm ($g_{SPK}$ = U(0,12) nS). (*F*) Example traces illustrating minimal changes in spike shape and (*G*) reduced spike threshold induced by a hyperpolarizing shift in the (in)activation dynamics of spike generating sodium currents ($I_{Na}$ & $I_{SPK}$). (*H*) Relationship between $g_{Tonic}$ and the percentage of the network in tonic or bursting modes during $I_{Na}$ & $I_{SPK}$ (in)activation hyperpolarization. (*I*) Number of burst-capable neurons in the simulated preBötC network as a function of $I_{Na}$ & $I_{SPK}$ (in)activation hyperpolarization. *Insets* show representative intrinsic burster. (*J*) Network rhythm during linear hyperpolarization of $I_{Na}$ & $I_{SPK}$ (in)activation. (*K*) Example traces comparing spike shape under control and simulated steady-state hypoxia ($I_{Na}$ = 47.5 mM, $\Delta V_{Na}^{1/2}$ = 1 mV). (*L*) Relationship between $g_{Tonic}$ and the percentage of the population in tonic or bursting modes showing net decrease in excitability and (*M*) an increased percentage of the network that is burst-capable during hypoxia. (*N*) Effect of hypoxia on a representative intrinsic burster. (*O*) Network rhythm during simulated transition to hypoxia. (*P*) Example network traces before (*i*) and during the augmenting (*ii*) and gasping (*iii*) phases of the hypoxic response. (*Q*) Network activity and (*R*) parameter space supporting network rhythmogenesis during progressive $I_{NaP}$ block under control (white) and hypoxic (purple) conditions.

excitability was reduced (Fig. 5*L*). In the network, the fraction of burst-capable neurons increased from 38% to 54% (Fig. 5*M*) and the firing rate and duration of intrinsic bursts also increased (Fig. 5*N*). When combined, the coupled network responded with an initial increase in spiking activity and burst frequency followed by a rapid transition to a slow gasping-like rhythm with a loss of preinspiratory spiking and transformation of the burst shape from symmetrical to decrementing (Fig. 5 *O* and *P*). Importantly, under these conditions, the network rhythm was also much more sensitive to $I_{NaP}$ suppression as demonstrated for the preBötC network in vitro (23). However, this was due to reduced excitability rather than an altered role of $I_{NaP}$ or intrinsic bursting, as network rhythms could be restarted by increasing excitability (Fig. 5 *Q* and *R*).

***Developmental Changes in Spike Shape and Intrinsic Bursting Mediated by Increasing Conductance Densities.*** Experimental investigations of preBötC rhythmogenesis and intrinsic bursting have largely been restricted to prenatal or neonatal development (8, 18, 21, 40, 42). The possibility that intrinsic bursting may be a preBötC feature restricted to early development, is a longstanding criticism of the pacemaker hypothesis. In general, during embryonic/postnatal development, spike amplitude and AHP increase, while duration decreases (38, 39). These changes result from increasing ion channel densities (38, 39, 43, 44). Thus, we scaled ionic conductances to predict how neurodevelopment may affect spike shape, intrinsic bursting, and network dynamics.

In single model neurons, we simulated neurodevelopment by applying a scaling factor ranging from 0.25X to 2.5X to all conductances except $g_{NaP}$ (Fig. 6*A*). When conductances were scaled down, spike amplitude and AHP were reduced and spike duration increased (Fig. 6*B*). At the same time, the magnitude of $g_{Tonic}$ required to generate spiking decreased and the spike "threshold" depolarized (*SI Appendix*, Fig. S9 *A* and *B*). Notably, further reducing spike amplitude and AHP by down-scaling conductances rendered them unable to generate sustained trains of spikes (Fig. 6*B*), as observed in early embryonic development (38). Conversely, as conductances were scaled up, spike amplitude and AHP increased, spike duration decreased, the magnitude of $g_{Tonic}$ required for spike generation increased and spike "threshold" hyperpolarized (Fig. 6 *B* and *C* and *SI Appendix*, Fig. S9 *A* and *B*). Among burst-capable neurons, conductance scaling transformed the shape of bursts, which resembled long-duration plateau-like bursters with down-scaling (40) and became shorter in duration with up-scaling until neurons transitioned to tonic spiking (Fig. 6*E*). Interestingly, the frequency range of these plateau-like bursters is very restricted (≈0.05 Hz to ≈0.1 Hz) and their bursting capabilities are highly insensitive to $I_{NaP}$ attenuation (*SI Appendix*, Fig. S10 *A* and *B*), consistent with experimental recordings (40).

To examine how concurrent neurodevelopmental changes in $g_{NaP}$ may affect intrinsic bursting and network dynamics, we added scaling to $g_{NaP}$ ranging from 0*X* to 2*X* the scaling factor applied to other voltage-gated conductances (m = 0 to 2, Fig. 6 *D*, *Inset*). In model networks ($g_{SPK}$ = U(0,12) nS), we quantified the proportion of burst-capable neurons as conductance densities undergo scaling with varied ratios of concurrent $g_{NaP}$ scaling (Fig. 6*D*). Simulations in networks with $g_{SPK}$ = 0, 6, or 12 are shown in *SI Appendix*, Fig. S11. In all cases, when conductances were low (scaling factor <0.5X), intrinsic bursting was not possible in any neurons. When $g_{NaP}$ was concurrently scaled,

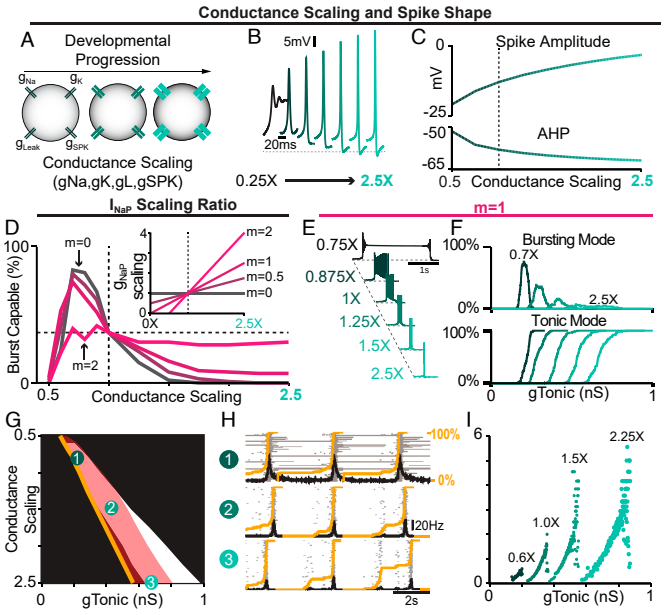


**Fig. 6.** Predicted developmental changes in spike shape, intrinsic bursting, and network dynamics due to changing conductance densities. (*A*) Illustration of conductance scaling during development. (*B*) Example traces and (*C*) quantification of spike amplitude and AHP as conductances are scaled. (*D*) percentage of the network ($g_{SPK}$ = U(0,12) nS) that is burst-capable as conductances are up- or down-scaled from control values (dashed vertical line). The *Inset* shows concurrent $g_{NaP}$ scaling ratio ($m$ = 0 to 2). (*E*) Example intrinsic bursting neurons during conductance scaling with $m$ = 1. (*F*) Decreased excitability with conductance scaling as indicated by a rightward shift in the level of $g_{Tonic}$ needed to initiate intrinsic bursting or tonic spiking. (*G*) Parameter space that supports intrinsic bursting (red) and network rhythmogenesis (white) as conductances are scaled. Orange lines indicate $g_{Tonic}$ where ≥1 neuron enters tonic spiking mode. (*H*) Raster plots and overlaid network firing rate corresponding to points 1 to 3 in (*G*) (Orange lines indicate the percentage of neurons active since the preceding network burst). (*I*) Relationship between $g_{Tonic}$ and network burst frequency as conductances are scaled.

the fraction of burst-capable neurons quickly increased with up-scaling, reaching a peak of ≈70 to 80% (≈38% for $m$ = 2) at a scaling factor of 0.75X, and then declining to 38% under control conditions (scaling factor = 1X). As conductance densities were further increased, the number of burst-capable neurons continued to decline until intrinsic bursting was lost or only possible in a small fraction of the population except for the case when $m$ = 2 where this decline was small (Fig. 6*D* and *SI Appendix*, Figs. S11*A* and S12*B*). This decline in intrinsic bursting typically corresponded with increasing preinspiratory spiking activity (Fig. 6*H* and *SI Appendix*, Fig. S12*D*), and also expanded the excitability ($g_{Tonic}$) range that supported rhythmogenesis, allowing a much wider range of network frequencies (Fig. 6*I* and *SI Appendix*, Fig. S12*E*). In all cases, rhythmogenesis remained $I_{NaP}$-dependent and, interestingly, intrinsic bursting became more sensitive to $I_{NaP}$ attenuation whereas network sensitivity was unchanged or slightly decreased (*SI Appendix*, Fig. S10*C*). These results illustrate that, even with scaling up of $g_{NaP}$, intrinsic bursting can remain limited to a subset of neurons within a certain developmental period, supporting the conclusion that intrinsic bursting is a nonessential feature of $I_{NaP}$-dependent network rhythm generation.

***In vitro to in vivo: impact of extracellular potassium and temperature on cellular and network bursting.*** Inherent in the process of creating the in vitro preBötC slice, excitatory inputs from regions outside the preBötC that regulate its activity are removed. To compensate for this loss of excitability, elevating the concentration of potassium in the bathing solution to between 8 and 9 mM is standard practice to promote reliable rhythmic activity from preBötC slices. In addition, slices are typically maintained at a subphysiological temperature (27 °C) to extend the viability of the preparation (2, 8, 18, 45). The possibility that these artificial conditions may also impact intrinsic bursting has been an enduring criticism of the pacemaker hypothesis and the in vitro preparation in general. Indeed, to what extent the biophysical mechanisms of rhythm generation seen under in vitro conditions are representative of normal physiology remains unclear and has been an important caveat common to the study of CPGs in general (1, 3). Because spike shape changes with both temperature (33) and extracellular potassium ($[K^+]_e$) (36, 37), we explored how these variables may impact intrinsic bursting and network rhythms to better understand whether the biophysical mechanisms of rhythm generation are conserved under simulated temperatures and $[K^+]_e$ associated with in vitro and in vivo conditions.

In single model neurons, reducing $[K^+]_e$ hyperpolarized the $K^+$ and leak reversal potentials ($E_K$ and $E_{Leak}$, *SI Appendix*, Fig. S13*A*), which increased the spike AHP and slightly reduced spike amplitude (Fig. 7 *A1* and *B1*), as expected (36, 37, 46). In the model preBötC network with distributed spike amplitudes ($g_{SPK}$ = U(0,12) nS), decreasing $[K^+]_e$ from a baseline value of 8.5 mM reduced excitability as indicated by an increased $g_{Tonic}$ required for neurons to enter spiking/bursting modes (Fig. 7*C1*). Additionally, decreasing $[K^+]_e$ quickly reduced and then eliminated burst-capable neurons at $[K^+]_e$ <5 mM (Fig. 7*D1*), consistent with experimental observations (20). Reducing $[K^+]_e$ below 5 mM also led to the cessation of the network rhythm (Fig. 7*E1*), as is typical in most in vitro preBötC slice preparations (2, 20, 29). However, if a source of excitatory drive was provided to the network to increase its excitability ($g_{Tonic}$), as expected to be present in vivo, the network rhythm re-emerged despite the continued absence of intrinsic bursting. Interestingly, at $[K^+]_e$ = 4 mM, the onset of simulated hypoxia (Fig. 5) revealed a transient rhythm that re-emerged and persisted following recovery from hypoxia (*SI Appendix*, Fig. S14*A*), as has been observed experimentally (47). In the model, this is due to short-term $[Na^+]_{in}$ dynamics and the long-lasting hyperpolarizing shift in the voltage-dependence of $I_{Na}$ (in)activation.

Next, we considered the potential consequences of temperature. Spike amplitude and AHP are known to decrease with increasing temperature (33) including in preBötC neurons (34). These changes are thought to be largely due to faster dynamics of voltage-gated channels and increased neuronal capacitance (33, 48). Therefore, to simulate changes in temperature, we added temperature dependence to voltage-dependent rate constants and cell capacitance such that all rate constants are reduced by ≈70% and capacitance increases by ≈1pf over the 10 °C change from 27 °C to 37 °C (*SI Appendix*, Fig. S13 *B* and *C*), see *Materials and Methods* . With these dependencies, simulating an increase in temperature decreased spike amplitude and AHP (Fig. 7 *A2* and *B2*), consistent with experimental observations (33). In the network, increasing temperature increased the possible number of neurons concurrently in a bursting mode but did not impact excitability as indicated by an unchanged $g_{Tonic}$ required to depolarize neurons into spiking/bursting modes (Fig. 7*C2*). Importantly, the number of burst-capable neurons was increased from 38% at 27 °C to 75% at 37 °C (Fig. 7*D2*) and interestingly, some neurons that were initially in a bursting mode

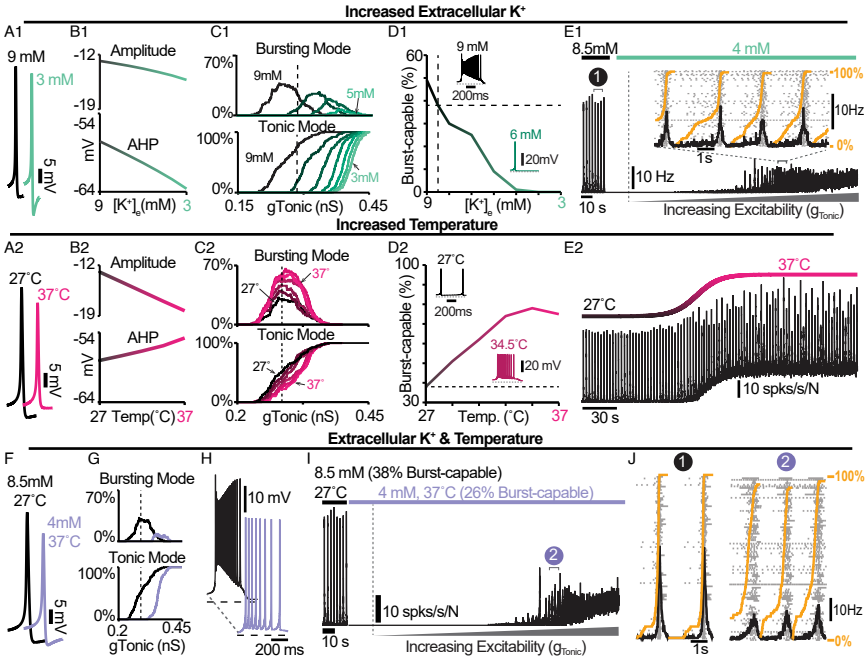


**Fig. 7.** Regulation of spike shape, intrinsic bursting, and network dynamics by $[K^+]_e$ and temperatures associated with in vitro and in vivo conditions. (*A1* and *A2*) Example traces and (*B1* and *B2*) quantified spike amplitude and AHP during changes in $[K^+]_e$ or temperature. (*C1* and *C2*) Relationship between $g_{Tonic}$ and the percentage of the network in bursting or tonic modes during changes in $[K^+]_e$ or temperature. Notice the reduced excitability at lower $[K^+]_e$ and increased excitability at higher temperatures. (*D1* and *D2*) Percentage of burst-capable neurons in the network as a function of $[K^+]_e$ or temperature with *Insets* of a representative intrinsic burster. (*E1*) Network rhythm at 8.5 mM and 4 mM $[K^+]_e$ during increasing $g_{Tonic}$. (*E2*) Network rhythm during an increase in temperature from 27 °C to 37 °C. (*F*) Example spike shapes under in vitro ($[K^+]_e$ = 8.5 mM, T = 27 °C) and in vivo-like ($[K^+]_e$ = 4 mM, T = 37 °C) conditions. (*G*) Relationship between $g_{Tonic}$ and the percentage of the population in bursting or tonic modes under in vivo-like conditions. (*H*) Representative intrinsic burster in each condition. (*I*) Network rhythm during transition from in vitro to in vivo $[K^+]_e$ and temperature with increasing excitatory drive ($g_{Tonic}$). (*J*) Rasters and overlaid population firing rate for points 1 and 2 shown in E1 and I (Orange lines indicate fraction of the network active since preceding burst).

transitioned to tonic spiking mode and vice versa, consistent with the findings of ref. 34 (*SI Appendix*, Fig. S13*D*). In the coupled network, this resulted in a shift in the baseline spiking activity of the network and an increase in burst frequency (Fig. 7*E2*), as observed experimentally (34, 49).

Finally, we examined how differences in $[K^+]_e$ and temperature may impact the cellular- and network-level properties of the preBötCin vitro and in vivo. In single model neurons, simultaneously decreasing $[K^+]_e$ from 8.5 to 4 mM and increasing temperature from 27 °C to 37 °C resulted in a net decrease in spike amplitude and AHP (Fig. 7*F*). In the network, this change in $[K^+]_e$ and temperature reduced excitability, requiring higher $g_{Tonic}$ for neurons to enter tonic/bursting modes, decreased the possible number of neurons concurrently in bursting mode, reduced the number of burst-capable neurons from 38% to 26%, and decreased spike frequency during bursts (Fig. 7 *G* and *H*). Despite the persistence of intrinsic bursting capabilities, this change in $[K^+]_e$ and temperature caused cessation of the network rhythm due to reduced excitability. If an excitatory input was applied to the network ($g_{Tonic}$) the network rhythm re-emerged (Fig. 7*I*). Under these conditions, the dynamic frequency range of the network remained largely unchanged or slightly reduced (*SI Appendix*, Fig. S15), and there was a higher fraction of the network participating in preinspiratory activity (Fig. 7*J*). Interestingly, in the model, if synaptic strength was increased at physiological $[K^+]_e$, as suggested by prior experiments (50), the network rhythm increased in amplitude and became more robust (*SI Appendix*, Fig. S13*E*). Despite the differences in cellular activity phenotypes network rhythmogenesis remained dependent on $I_{NaP}$ under all conditions (*SI Appendix*, Fig. S13*F*).

## Discussion

This study addresses a longstanding debate surrounding respiratory rhythmogenesis using computational modeling to disentangle the conflated role(s) of $I_{NaP}$ and intrinsic bursting. We find that small changes in spike shape can interact with $I_{NaP}$ gating dynamics to transition neurons from bursting to tonic spiking and render them incapable of intrinsic bursting (Fig. 1). In an established preBötC network model that is commonly viewed as a quantitative realization of the pacemaker hypothesis, we leverage this interaction to selectively render all neurons capable or incapable of intrinsic bursting. By doing so, we demonstrate that preBötC rhythmogenesis persists in both extremes—when intrinsic bursting is not possible and neurons exhibit intrinsically tonic activity associated with preinspiratory spiking in the network, and also when all neurons are capable of intrinsic bursting but the network lacks preinspiratory spiking. (Fig. 2). Thus, while these phenotypes of preBötC neurons may be present and reflect degenerate modes of rhythm generation, they are conditional and are not, on their own, essential elements for rhythmogenesis. Instead, regardless of the amount of intrinsic bursting or preinspiratory spiking, rhythmogenesis per se remains dependent on interactions between $I_{NaP}$ and recurrent synaptic excitation (Figs. 3–4). Consistent with these findings, we illustrate how conditional factors that impact spike shape including oxygenation (Fig. 5), development (Fig. 6), extracellular potassium, and temperature (Fig. 7) can substantially alter the relative abundance of intrinsic bursting and preinspiratory spiking without precluding rhythm generation. Rather than being rhythmogenic, we propose that these dynamic activity phenotypes of preBötC neurons are a feature of a degenerate network that evolved to be robust, ensuring breathing persists despite developmental or environmental changes, while remaining able to accommodate the wide range of breathing patterns associated with its physiological, behavioral, and emotional integration (51, 52).

Over the last three decades, the debate surrounding preBötC rhythmogenesis has remained largely unchanged, stemming, in part, from the simplistic framing of the pacemaker and group-pacemaker/burstlet theories. Although attractive and broadly accessible, this simplicity supports a false dichotomy rooted in necessity/sufficiency criterion that obscures more nuanced interpretations critical to achieve a consensus view.

First, it implies that these theories are mutually exclusive. For example, in group-pacemaker-based interpretations,

rhythmogenesis is described as an "emergent" property of the network because it arises from interactions among "nonrhythmic" intrinsically tonic neurons. On the other hand, in networks that contain intrinsically bursting neurons, rhythmicity is often assumed to be driven by the activity of these bursting neurons as if they were "pacing" the network. However, intrinsic burst frequencies are quite variable (17) and, as with any other preBötC neuron, pacemaker neurons are embedded within a recurrently connected network. Accordingly, synaptic interactions are always required to coordinate cellular activity into a coherent network rhythm regardless of the intrinsic spiking patterns of its constituent neurons (Fig. 3), and therefore all network rhythms are "emergent." Moreover, tonic spiking and intrinsic bursting are both rhythmic processes, and the synchronization of individual spikes or clusters of spikes (i.e. bursts) across the network via synaptic interactions may share far more similarities than differences. Indeed, in the model presented here, we find that the initiation of network bursts depends on both $I_{NaP}$ activation and recurrent excitatory interactions, whereas $I_{NaP}$ inactivation and synaptic depression both contribute to burst termination (Fig. 3). Thus, the roles of network interactions and the intrinsic properties of the neurons within it should not be considered separable or "one or the other." Instead, we propose that "the" mechanism of rhythm generation involves multiple interacting and interdependent properties of the preBötC.

Second, with this framing, $I_{NaP}$ has become misconstrued with intrinsic bursting and the pacemaker hypothesis. This may reflect, in part, the way in which intrinsic bursting and $I_{NaP}$ were initially characterized in the preBötC—first with the discovery of pacemaker neurons (2), followed by incorporation of $I_{NaP}$ into computational models with the goal of replicating the pacemaker phenotype (7), and finally subsequent experimental confirmation of $I_{NaP}$ expression and $I_{NaP}$-dependent pacemaker neurons in the preBötC (8, 18). This progression of discovery strongly supported the assumption that the purpose of $I_{NaP}$ in the preBötC is to endow some neurons with intrinsic bursting properties, which in turn drives rhythmic activity of the network. However, rather than a driver of rhythm, our findings suggest that it may be more accurate to view intrinsic bursting as a consequence of $I_{NaP}$-dependent rhythm generation that is only possible in neurons that happen to have a certain combination of properties including, but not limited to, $g_{NaP}$, $g_{Leak}$, and any of the many properties that influence spike shape (33–39), see Figs. 2–7. Taking this view, one need not consider the small subset of neurons that are capable of intrinsic bursting to be a specialized cell type with a unique functional role in rhythm generation. Indeed, our simulations demonstrating that blockade of $I_{NaP}$ specifically in burst-capable or incapable neurons has similar consequences for the network rhythm (Fig. 4) support this view. It is also consistent with experimental observations that the preBötC rhythm can persist even after intrinsic bursting is apparently abolished by pharmacological or genetic attenuation of $I_{NaP}$ (9, 16). Due to the conflation of $I_{NaP}$ and intrinsic bursting, these findings have reinforced the idea that $I_{NaP}$ is not obligatory for preBötC rhythm generation. However, our simulations clearly illustrate that $I_{NaP}$ can be critical for rhythm generation independent of any requirement for intrinsic bursting (Figs.2 and 3), and that $I_{NaP}$-dependent preBötC rhythms can persist long after intrinsic bursting has been abolished by partial $I_{NaP}$ block (Figs. 4 and 5, *SI Appendix*, Fig. S6, S7 *E1–E3*, S10*C*, and S13*F*), providing an important proof of concept that equating $I_{NaP}$ and intrinsic bursting is an oversimplification.

The debate surrounding the role of $I_{NaP}$ has also been exacerbated by the seemingly inconsistent effects of $I_{NaP}$ blockers. (8, 18, 23, 42, 45). For example, in cases where $I_{NaP}$ antagonists have failed to eliminate the preBötC rhythm, proponents of the pacemaker hypothesis often contend that this is because $I_{NaP}$ block was incomplete due to insufficient diffusion of drug into the tissue (14, 18, 53). In contrast, in cases where $I_{NaP}$ blockers have eliminated the preBötC rhythm, proponents of group pacemaker/burstlet theory, generally attribute this to $I_{NaP}$'s contribution to excitability rather than rhythmogenesis (42). This is supported by observations that, following elimination of the preBötC rhythm with the $I_{NaP}$ blocker Riluzole, rhythmicity could be restored by application of substance P to increase preBötC excitability (42). Here, we illustrate how $I_{NaP}$'s contribution to preBötC excitability can be a key factor underlying the widely variable responses of the preBötC rhythm to suppression of $I_{NaP}$ (Fig. 4), providing a plausible explanation for these apparently discrepant findings. Because sufficient excitability is required for preBötC rhythmogenesis, if the level of excitability is initially low, a modest suppression of $I_{NaP}$ ($\lesssim$10%) will quickly stop the rhythm due a reduction in excitability. However, if baseline excitability is higher, it becomes much more difficult for $I_{NaP}$ suppression to stop the rhythm. Further, once the rhythm has been stopped by partial suppression of $I_{NaP}$, it can be restarted by increasing excitability so long as $I_{NaP}$ has not been suppressed by more than 80 to 85%, consistent with experiments suggesting that the preBötC rhythm can only be restarted when $I_{NaP}$ block is incomplete (14, 18). Thus, the wide variation in the sensitivity of the preBötC rhythm to suppression of $I_{NaP}$ does not indicate that $I_{NaP}$ has a more important rhythmogenic role in one condition vs. another. Nor does the ability to recover rhythmicity by increasing excitability suggest that $I_{NaP}$ is not an essential element of rhythmogenesis. Instead, independent from its contribution to excitability, $I_{NaP}$ remains important for rhythm generation due to its contributions to burst initiation and termination (Fig. 3), consistent with optogenetic manipulations of preBötC excitability during graded pharmacological block of $I_{NaP}$ (14). Notably, the prevalence of burst-capable neurons in the network has little effect on the relationship between excitability and the sensitivity of the rhythm to $I_{NaP}$ suppression (Fig. 4 and *SI Appendix*, Figs. S6 and S7*D*). Collectively, these simulations illustrate that $I_{NaP}$'s role in preBötC rhythmogenesis is not limited to its contribution to excitability or intrinsic bursting, and provide important conceptual insight into why experimental efforts to define the role of $I_{NaP}$ in preBötC rhythm generation have been inconsistent and difficult to interpret.

Third, both theories generally overlook the conditional nature of intrinsic bursting and preinspiratory spiking (3–5). Importantly, our simulations reveal an inverse relationship between the prevalence of intrinsic bursting and preinspiratory spiking that can be profoundly altered by small changes in spike shape. A long-standing critique of the pacemaker hypothesis (and by association $I_{NaP}$) is the lack of evidence for intrinsic bursting in adult animals in vivo, suggesting that intrinsic bursting is restricted to early development and/or the artificial conditions used in vitro. Here, we illustrate how these conditional factors can shift the prevalence of intrinsic bursting and preinspiratory spiking without altering the role of $I_{NaP}$ in rhythmogenesis.

In vitro and in vivo experiments are typically performed at different $[K^+]_e$ and temperature. In preBötC slices, artificially increasing $[K^+]_e$ promotes rhythmogenesis and also intrinsic bursting (20). In contrast, lower $[K^+]_e$ (sometimes with altered

[$Ca^{2+}$]) promotes weaker "burstlet" rhythms hypothesized to be driven by preinspiratory spiking rather than intrinsic bursting or $I_{NaP}$ (3). Consistent with these experimental observations, lowering $[K^+]_e$ in the model reduces the number of burst-capable neurons in the network due to an increase in spike AHP. Experimentally, at physiological $[K^+]_e$, intrinsic bursting is eliminated and the network rhythm stops (20). However, the latter is a consequence of reduced cellular excitability because rhythmogenesis can be restored if excitatory drive is increased (Fig. 7), as is expected in vivo due to the presence of e.g. neuromodulatory and chemoreceptor inputs. Under these conditions, intrinsic bursting remains absent and preinspiratory spiking is increased (Fig. 7). However, another artificial aspect of in vitro experiments is low temperature, which has an inverse relationship with spike amplitude and AHP (33); Fig. 7. Warmer temperatures in vivo are therefore expected to counteract the effects of low $[K^+]_e$ on intrinsic bursting. As a result, our model predicts that at physiological temperature and $[K^+]_e$ some neurons remain burst-capable, consistent with experiments that have identified intrinsic bursting preBötC neurons at physiological $[K^+]_e$ but at slightly warmer temperatures (30 °C to 31 °C) (24, 54).

In vitro and in vivo experiments are generally performed at different stages of development. Intrinsic bursting in the preBötC is often thought to be most prevalent during early development (40), and attempts to record rhythmic preBötC activity in slices from rodents $\lesssim$P14 have been generally unsuccessful. This has reinforced the idea that intrinsic bursting drives rhythmic activity of the preBötC in vitro and that the preBötC rhythm in vivo must be generated by a distinct mechanism such as reciprocal inhibition (5). Our simulations illustrate how the abundance of burst-capable neurons can peak during early development due to changes in spike shape that are expected as the densities of channel conductances increase (38, 39); Fig. 6. However, this change in the abundance of burst-capable neurons does not represent a shift in the underlying rhythmogenic elements of the network. Instead, an increasing amount of excitatory drive becomes required for rhythmogenesis as neurodevelopment progresses (Fig. 6), which may contribute to the difficulties associated with generating rhythmic preBötC slices beyond this early developmental period.

Collectively, these factors may help explain the lack of evidence for intrinsically bursting preBötC neurons in vivo. However, a major conclusion of our study is that intrinsic bursting is not a prerequisite for $I_{NaP}$-dependent rhythmogenesis (Figs. 2 and 4). Therefore, even if preBötC neurons are not capable of intrinsic bursting in vivo, this does not indicate that $I_{NaP}$ isn't an important feature of preBötC rhythmogenesis. To the contrary, the conceptual insights of our study support the hypothesis that the preBötC utilizes the same cellular and network properties for rhythm generation in vivo vs. in vitro, during hypoxia, and at different stages of neurodevelopment. However, the network is able to produce degenerate modes of rhythm generation by developmentally and/or conditionally altering the abundance of intrinsic bursting/preinspiratory spiking phenotypes, characteristics of the network rhythm (frequency, amplitude, shape), and the amount of excitability required for rhythmogenesis through modest changes in spike shape. Conditions associated with less intrinsic bursting and more preinspiratory spiking generally result in a more dynamic preBötC network that is able to produce a wider range of frequencies with relatively small changes in excitatory input (Figs. 2, 6, and 7). From a teleological perspective, it may make sense for activity phenotypes of preBötC neurons to transition away from intrinsic bursting as development progresses and breathing becomes integrated with an increasingly complex repertoire of nonrespiratory functions such as sniffing, vocalizing, nociception, emotion, and swallowing. Breathing in vivo must also be easily stopped and started, e.g. breath hold, and such changes in the preBötC may ensure it continues to operate near this phase transition with sufficient gain to allow optimal responses to internal and external inputs.

The parameters of our model are based on available data. However, computational models are always limited by approximations and cannot include all biological variables. Indeed, additional biophysical properties such as network topology, synaptic weight distributions, synaptic facilitation, synaptic inhibition, and various currents not captured by this model may also play important role(s) in burst initiation and/or termination under some conditions. For example, when computational models of the preBötC, similar to this one, are expanded to include inhibitory neurons, rhythmogenesis may be sustained by reciprocal network interactions and/or $I_{NaP}$ in a state-dependent manner (53). Similarly, in the current study, we do not know how each individual conductance scales with development, or whether time constants for each voltage-gated parameter are similarly affected by temperature. However, the important conceptual takeaways hold true across different permutations and simulations. 1) Due to interaction with the voltage-dependent properties of $I_{NaP}$, anything that alters spike shape can influence intrinsic bursting. 2) Interacting cellular ($g_{NaP}$ and excitability) and network (excitatory synaptic interactions) properties form the inexorable substrate for rhythm generation, whereas the activity patterns of individual neurons are conditional phenotypes that reflect changes in network "states" rather than changes in rhythmogenic mechanism. And, 3) modulation of spike shape can have important consequences for rhythm characteristics and network flexibility. Because $I_{NaP}$ is widely expressed in the brain (55–58) and is a feature of many CPGs, the conceptual insights of our study may provide a useful framework for understanding many different forms of brain rhythmicity.

## Materials and Methods

Model neurons incorporate Hodgkin–Huxley style conductances as described in previous studies (14, 15, 27, 53). The currents include action potential generating $Na^+$ and delayed rectifying $K^+$ currents ($I_{Na}$ and $I_K$), a persistent $Na^+$ current ($I_{NaP}$), a voltage-gated $Ca^{2+}$ current ($I_{Ca}$), a $K^+$ dominated leak current ($I_{Leak}$), a tonic excitatory synaptic current ($I_{Tonic}$) and a dynamic excitatory synaptic current ($I_{Syn}$) which mediates network interactions. The high voltage-activated currents, $I_{SPK}$ and $I_{AHP}$, were added to manipulate spike amplitude and AHP. Networks contain N=100 neurons with 13% connection probability. Full details of the computational model are given in *SI Appendix*.

**Data, Materials, and Software Availability.** All study data are included in the article and/or *SI Appendix* (59).

**ACKNOWLEDGMENTS.** This work was supported by NIH grants R01 HL166317 (N.A.B.), R00 HL145004 (N.A.B.) and K01 1K01DA058543-01 (R.S.P.).

Author affiliations: [a]Center for Integrative Brain Research, Seattle Children's Research Institute, Seattle, WA 98101; [b]Pulmonary, Critical Care and Sleep Medicine, Department of Pediatrics, University of Washington, Seattle, WA 98195; and [c]Department of Physiology and Biophysics, University of Washington, Seattle, WA 98195

1. J. M. Goaillard, E. Marder, Ion channel degeneracy, variability, and covariation in neuron and circuit resilience. *Annu. Rev. Neurosci.* **44**, 335–357 (2021).
2. J. C. Smith, H. H. Ellenberger, K. Ballanyi, D. W. Richter, J. L. Feldman, Pre-bötzinger complex: A brainstem region that may generate respiratory rhythm in mammals. *Science* **254**, 726–729 (1991).
3. J. L. Feldman, K. Kam, Facing the challenge of mammalian neural microcircuits: Taking a few breaths may help. *J. Physiol.* **593**, 3–23 (2015).
4. J. M. Ramirez, N. A. Baertsch, The dynamic basis of respiratory rhythm generation: One breath at a time. *Annu. Rev. Neurosci.* **41**, 475–499 (2018).
5. J. C. Smith *et al*., Respiratory rhythm generation in neonatal and adult mammals: The hybrid pacemaker-network model. *Resp. Physiol.* **122**, 131–147 (2000).
6. J. C. Rekling, J. L. Feldman, PreBötzinger complex and pacemaker neurons: Hypothesized site and kernel for respiratory rhythm generation. *Annu. Rev. Physiol.* **60**, 385–405 (1998).
7. R. J. Butera, J. Rinzel, J. C. Smith, Models of respiratory rhythm generation in the pre-Botzinger complex. I. Bursting pacemaker neurons. *J. Neurophysiol.* **82**, 382–397 (1999).
8. C. A. Del Negro, N. Koshiya, R. J. Butera Jr, J. C. Smith, Persistent sodium current, membrane properties and bursting behavior of pre-botzinger complex inspiratory neurons in vitro. *J. Neurophysiol.* **88**, 2242–2250 (2002).
9. C. A. Del Negro, C. Morgado-Valle, J. L. Feldman, Respiratory rhythm: An emergent network property? *Neuron* **34**, 821–830 (2002).
10. R. W. Pace, D. D. Mackay, J. L. Feldman, C. A. Del Negro, Inspiratory bursts in the prebötzinger complex depend on a calcium-activated non-specific cation current linked to glutamate receptors in neonatal mice. *J. Physiol.* **582**, 113–125 (2007).
11. H. Koizumi *et al*., Transient receptor potential channels TRPM4 and TRPC3 critically contribute to respiratory motor pattern formation but not rhythmogenesis in rodent brainstem circuits. *Eneuro* **5** (2018).
12. M. C. D. Picardo *et al*., Trpm4 ion channels in pre-bötzinger complex interneurons are essential for breathing motor pattern but not rhythm. *PLoS Biol.* **17**, e2006094 (2019).
13. X. Sun *et al*., Opioids modulate an emergent rhythmogenic process to depress breathing. *Elife* **8**, e50613 (2019).
14. R. S. Phillips, H. Koizumi, Y. I. Molkov, J. E. Rubin, J. C. Smith, Predictions and experimental tests of a new biophysical model of the mammalian respiratory oscillator. *Elife* **11**, e74762 (2022).
15. R. S. Phillips, J. E. Rubin, Putting the theory into "burstlet theory" with a biophysical model of burstlets and bursts in the respiratory prebötzinger complex. *Elife* **11** (2022).
16. C. A. da Silva, C. J. Grover, M. C. D. Picardo, C. A. Del Negro, Role of nav1.6-mediated persistent sodium current and bursting-pacemaker properties in breathing rhythm generation. *Cell Rep.* **42**, 113000 (2023).
17. S. M. Johnson, J. C. Smith, G. D. Funk, J. L. Feldman, Pacemaker behavior of respiratory neurons in medullary slices from neonatal rat. *J. Neurophysiol.* **72**, 2598–2608 (1994).
18. H. Koizumi, J. C. Smith, Persistent na+ and k+-dominated leak currents contribute to respiratory rhythm generation in the pre-bötzinger complex in vitro. *J. Neurosci.* **28**, 1773–1785 (2008).
19. R. J. Butera, J. Rinzel, J. C. Smith, Models of respiratory rhythm generation in the pre-botzinger complex. II. Populations of coupled pacemaker neurons. *J. Neurophysiol.* **82**, 398–415 (1999).
20. C. A. Del Negro, S. M. Johnson, R. J. Butera, J. C. Smith, Models of respiratory rhythm generation in the pre-botzinger complex. III. Experimental tests of model predictions. *J. Neurophysiol.* **86**, 59–74 (2001).
21. K. Ptak *et al*., Sodium currents in medullary neurons isolated from the pre-bötzinger complex region. *J. Neurosci.* **25**, 5159–5170 (2005).
22. F. Peña, J. M. Ramirez, Endogenous activation of serotonin-2a receptors is required for respiratory rhythm generation in vitro. *J. Neurosci.* **22**, 11055–11064 (2002).
23. F. Peña, M. A. Parkis, A. K. Tryba, J. M. Ramirez, Differential contribution of pacemaker properties to the generation of respiratory rhythms during normoxia and hypoxia. *Neuron* **43**, 105–117 (2004).
24. A. K. Tryba, F. Peña, J. M. Ramirez, Stabilization of bursting in respiratory pacemaker neurons. *J. Neurosci.* **23**, 3538–3546 (2003).
25. R. A. Krey, A. M. Goodreau, T. B. Arnold, C. A. Del Negro, Outward currents contributing to inspiratory burst termination in prebötzinger complex neurons of neonatal mice studied in vitro. *Front. Neural Circuit.* **4**, 124 (2010).
26. L. D. Plant, J. D. Marks, S. A. Goldstein, Sumoylation of nav1. 2 channels mediates the early response to acute hypoxia in central neurons. *Elife* **5**, e20054 (2016).
27. R. S. Phillips, T. T. John, H. Koizumi, Y. I. Molkov, J. C. Smith, Biophysical mechanisms in the mammalian respiratory oscillator re-examined with a new data-driven computational model. *Elife* **8**, e41555 (2019).
28. N. A. Baertsch, N. E. Bush, N. J. Burgraff, J. M. Ramirez, Insights into the dynamic control of breathing revealed through cell-type-specific responses to substance P. *Elife* **8**, e51350 (2019).
29. P. S. Kallurkar, C. Grover, M. C. D. Picardo, C. A. Del Negro, Evaluating the Burstlet theory of inspiratory rhythm and pattern generation. *Eneuro* **7** (2020).
30. N. A. Baertsch, N. E. Bush, N. J. Burgraff, J. M. Ramirez, Dual mechanisms of opioid-induced respiratory depression in the inspiratory rhythm-generating network. *Elife* **10**, e67523 (2021).
31. J. E. Rubin, J. A. Hayes, J. L. Mendenhall, C. A. Del Negro, Calcium-activated nonspecific cation current and synaptic depression promote network-dependent burst oscillations. *Proc. Natl. Acad. Sci. U.S.A.* **106**, 2939–2944 (2009).
32. C. Guerrier, J. A. Hayes, G. Fortin, D. Holcman, Robust network oscillations during mammalian respiratory rhythm generation driven by synaptic dynamics. *Proc. Natl. Acad. Sci. U.S.A.* **112**, 9728–9733 (2015).
33. Y. Yu, A. P. Hill, D. A. McCormick, Warm body temperature facilitates energy efficient cortical action potentials. *PLoS Comput. Biol.* **8**, e1002456 (2012).
34. A. K. Tryba, J. M. Ramirez, Hyperthermia modulates respiratory pacemaker bursting properties. *J. Neurophysiol.* **92**, 2844–2852 (2004).
35. M. Gruss *et al*., Moderate hypoxia influences excitability and blocks dendrotoxin sensitive k+ currents in rat primary sensory neurones. *Mol. Pain* **2**, 1744–8069 (2006).
36. U. Strauss *et al*., Increasing extracellular potassium results in subthalamic neuron activity resembling that seen in a 6-hydroxydopamine lesion. *J. Neurophysiol.* **99**, 2902–2915 (2008).
37. J. J. Yang, R. C. Huang, Afterhyperpolarization potential modulated by local [k+] o in k+ diffusion-restricted extracellular space in the central clock of suprachiasmatic nucleus. *Biomed. J.* (2022).
38. B. X. Gao, L. Ziskind-Conhaim, Development of ionic currents underlying changes in action potential waveforms in rat spinal motoneurons. *J. Neurophysiol.* **80**, 3047–3061 (1998).
39. M. Fry, Developmental expression of na+ currents in mouse Purkinje neurons *Euro. J. Neurosci.* **24**, 2557–2566 (2006).
40. M. Chevalier, N. Toporikova, J. Simmers, M. Thoby-Brisson, Development of pacemaker properties and rhythmogenic mechanisms in the mouse embryonic respiratory network. *Elife* **5**, e16125 (2016).
41. J. A. Hellas, R. D. Andrew, Neuronal swelling: A non-osmotic consequence of spreading depolarization. *Neurocrit. Care* **35**, 112–134 (2021).
42. R. W. Pace, D. D. Mackay, J. L. Feldman, C. A. Del Negro, Role of persistent sodium current in mouse prebötzinger complex neurons and respiratory rhythm generation. *J. Physiol.* **580**, 485–496 (2007).
43. J. R. Huguenard, O. P. Hamill, D. A. Prince, Developmental changes in na+ conductances in rat neocortical neurons: Appearance of a slowly inactivating component *J. Neurophysiol.* **59**, 778–795 (1988).
44. F. Valiullina *et al*., Developmental changes in electrophysiological properties and a transition from electrical to chemical coupling between excitatory layer 4 neurons in the rat barrel cortex. *Front. Neural Circuit.* **10**, 1 (2016).
45. J. C. Smith, A. Abdala, H. Koizumi, I. A. Rybak, J. F. Paton, Spatial and functional architecture of the mammalian brain stem respiratory network: A hierarchy of three oscillatory mechanisms. *J. Neurophysiol.* **98**, 3370–3387 (2007).
46. M. U. Abdulla, R. S. Phillips, J. E. Rubin, Dynamics of ramping bursts in a respiratory neuron model. *J. Comput. Neurosci.* (2021).
47. S. L. Mironov, Calmodulin and calmodulin kinase ii mediate emergent bursting activity in the brainstem respiratory network (prebötzinger complex). *J. Physiol.* **591**, 1613–1630 (2013).
48. M. Plaksin, E. Shapira, E. Kimmel, S. Shoham, Thermal transients excite neurons through universal intramembrane mechanoelectrical effects. *Phys. Rev. X* **8**, 011043 (2018).
49. A. K. Tryba, J. M. Ramirez, Response of the respiratory network of mice to hyperthermia. *J. Neurophysiol.* **89**, 2975–2983 (2003).
50. K. C. Gonzalez, A. Losonczy, A. Negrean, Dendritic excitability and synaptic plasticity in vitro and in vivo. *Neuroscience*, S0306–4522 (2022).
51. J. W. Arthurs, A. J. Bowen, R. D. Palmiter, N. A. Baertsch, Parabrachial tachykinin1-expressing neurons involved in state-dependent breathing control. *Nat. Commun.* **14**, 963 (2023).
52. S. Ashhad, K. Kam, C. A. Del Negro, J. L. Feldman, Breathing rhythm and pattern and their influence on emotion. *Annu. Rev. Neurosci.* **45**, 223–247 (2022).
53. R. S. Phillips, J. E. Rubin, Effects of persistent sodium current blockade in respiratory circuits depend on the pharmacological mechanism of action and network dynamics. *PLoS Comput. Biol.* **15**, e1006938 (2019).
54. W. M. St.-John, R. L. Stornetta, P. G. Guyenet, J. F. Paton, Location and properties of respiratory neurones with putative intrinsic bursting properties in the rat in situ. *J. Physiol.* **587**, 3175–3188 (2009).
55. H. Su, G. Alroy, E. D. Kirson, Y. Yaari, Extracellular calcium modulates persistent sodium current-dependent burst-firing in hippocampal pyramidal neurons. *J. Neurosci.* **21**, 4173–4182 (2001).
56. J. C. Brumberg, L. G. Nowak, D. A. McCormick, Ionic mechanisms underlying repetitive high-frequency burst firing in supragranular cortical neurons. *J. Neurosci.* **20**, 4829–4843 (2000).
57. C. Alzheimer, P. C. Schwindt, W. E. Crill, Postnatal development of a persistent na+ current in pyramidal neurons from rat sensorimotor cortex *J. Neurophysiol.* **69**, 290–292 (1993).
58. A. Taddese, B. P. Bean, Subthreshold sodium current from rapidly inactivating sodium channels drives spontaneous firing of tuberomammillary neurons. *Neuron* **33**, 587–600 (2002).
59. R. Phillips, N. Baertsch, Interdependence-of-cellular-and-network-properties-in-respiratory-rhythm-generation. GitHub. https://github.com/RyanSeanPhillips/Interdependence-of-cellular-and-network-properties-in-respiratory-rhythm-generation. Deposited 18 September 2023.